Journal of Applied Physics

RESEARCH ARTICLE | FEBRUARY 09 2024

Decomposition characteristics of C_4F_7N-based SF_6-alternative gas mixtures

Wenqiang Gao ; Luisa Posada ; Vahid Shiravand ; Shubhashish Shubhashish ; Capri Price ; Boya Zhang ; Radislav Potyrailo; Karim Younsi; Shiyao Shan ; Ibrahima Ndiaye; Charlotte Cabrera; Jierui Zhou; Maxime Perret ; Thomas Berteloot; Yannick Kieffel; Andres Laso ; Nenad Uzelac; Steven L. Suib ; Yang Cao

J. Appl. Phys. 135, 063302 (2024)
https://doi.org/10.1063/5.0188478
CHORUS

AIP Publishing

Journal of Applied Physics ARTICLE pubs.aip.org/aip/jap

Decomposition characteristics of C_4F_7N-based SF_6-alternative gas mixtures

Cite as: J. Appl. Phys. **135**, 063302 (2024); doi: 10.1063/5.0188478
Submitted: 21 November 2023 · Accepted: 20 January 2024 ·
Published Online: 9 February 2024

Wenqiang Gao,[1,2] Luisa Posada,[3] Vahid Shiravand,[1,2] Shubhashish Shubhashish,[3] Capri Price,[4] Boya Zhang,[5] Radislav Potyrailo,[6] Karim Younsi,[6] Shiyao Shan,[6] Ibrahima Ndiaye,[6] Charlotte Cabrera,[7] Jierui Zhou,[1,2] Maxime Perret,[8] Thomas Berteloot,[8] Yannick Kieffel,[8] Andres Laso,[9] Nenad Uzelac,[9] Steven L. Suib,[3] and Yang Cao[1,2,a)]

AFFILIATIONS

[1]Department of Electrical and Computer Engineering, University of Connecticut, Storrs, Connecticut 06269, USA
[2]Electrical Insulation Research Center, Institute of Materials Science, University of Connecticut, Storrs, Connecticut 06269, USA
[3]Department of Chemistry, University of Connecticut, Storrs, Connecticut 06269, USA
[4]Institute of Materials Science, University of Connecticut, Storrs, Connecticut 06269, USA
[5]State Key Laboratory of Electrical Insulation and Power Equipment, Xi'an Jiaotong University, No. 28 XianNing West Road, Xi'an, Shaanxi Province 710049, China
[6]GE Global Research Center, Niskayuna, New York 12309, USA
[7]École Nationale Supérieure des Ingénieurs en Arts Chimiques et Technologiques, Toulouse 31030, France
[8]General Electric, Grid Solutions SAS, Villeurbanne 69100, France
[9]G&W Electric Company, 305 West Crossroads Pkwy, Bolingbrook, Illinois 60440, USA

[a)]**Author to whom correspondence should be addressed:** yang.cao@uconn.edu

ABSTRACT

C_4F_7N [2,3,3,3-tetrafluoro-2-(trifluoromethyl)propanenitrile]/CO_2 gas mixtures are being developed as an eco-friendly electrical insulator to replace SF_6, the most potent greenhouse industrial gaseous dielectric. However, recent studies have reported complicated and often conflicting decomposition pathways for C_4F_7N/CO_2 gas mixtures, which has raised concerns. In this work, the decomposition characteristics of C_4F_7N/CO_2 gas mixtures were studied comprehensively by both designed computations and experiments. Computations were performed starting from fundamental propositions of C_4F_7N/CO_2 decompositions, which were further experimentally verified by pyrolysis, long-term thermal aging with/without catalytic materials (industrial-grade molecular sieves 4A), and electrical decomposition by spark discharge. The results of both computations and experiments suggest that in an ideal thermal decomposition, C_4F_7N is likely to decompose into C_2F_6 and small fluoronitriles first at high temperatures. The generation of C_3F_6 and C_2N_2 from C_4F_7N thermal decomposition at lower temperatures appears because of the catalytic effect of incompatible materials, for example, the industrial-grade molecular sieves 4A that we tested. The electron impact dissociation of C_4F_7N plays an important role in C_4F_7N electrical decomposition, leading to additional formation of distinctive small molecules of CF_4 and C_2N_2 of low concentrations. It was pointed out based on a real arcing test in a load disconnector that the decomposition of C_4F_7N gas mixtures in real applications will be at a much moderate and manageable rate than what was obtained from the highly accelerated laboratory tests presented in this work. The signatures of decomposition products extracted in this study provide invaluable guidance for developing decomposition-based diagnosis and fixation of decomposition byproducts toward SF_6-free power grids.

I. INTRODUCTION

SF_6 has been widely used in modern power grids because of its outstanding high-voltage insulating and arc-quenching characteristics.[1] SF_6 is non-flammable, non-toxic, and chemically inert and tends to recombine to its original molecular structure after dissociation, which offers the highest reliability with the most compact design

options in gas-insulated systems. However, SF_6 is also the most potent industrial greenhouse gas with an extremely high global warming potential (GWP) of 23 500, and the increasing awareness of the environmental impact of SF_6 mandates its replacement.[2–6] After years of collective work, C_4F_7N [2,3,3,3-tetrafluoro-2-(trifluoromethyl)propanenitrile]/CO_2 gas mixtures have been identified as one of the most promising SF_6 alternatives for their combined strengths and balanced properties,[7–12] and a scaling-up adoption of C_4F_7N/CO_2 gas mixtures at the grid level is around the corner. Nevertheless, recent studies have reported complicated and often conflicting decomposition pathways for C_4F_7N/CO_2 gas mixtures, which have also raised concerns.[13–20]

In principle, gas molecules start to decompose once the energy input exceeds the energy barrier along one of their decomposition pathways, where the level of the energy input is highly related to the form of the input energy, and the energy barrier is influenced by catalysts. Based on the forms of the input energy, C_4F_7N/CO_2 decomposition can be divided into two major categories, namely, thermal decomposition and electrical decomposition. For C_4F_7N/CO_2 thermal decomposition, since the input energy is mainly in the form of heat, a local thermodynamic equilibrium (LTE) can be assumed for gas mixtures to be decomposed, and the decomposition characteristics of gas mixtures in such a state should comply with reaction kinetics developed in the framework of thermodynamics. For C_4F_7N/CO_2 non-arcing electrical decomposition, the energy input is mainly realized by the abundant hot electrons significantly away from the equilibrium state, and more possible decomposition reactions could be initiated.[16,20] Up until now, notable discrepancies in C_4F_7N/CO_2 decomposition characteristics have been reported even when tested with the same form of energy input. For example, while some thermal decomposition studies reported that C_4F_7N/CO_2 gas mixtures remained stable until 650 °C,[13] other studies reported that C_4F_7N started to decompose at temperatures down to 350 °C, or even lower, where C_3F_6 was likely to be generated first, followed by the generation of C_2N_2.[18] Furthermore, existing computational studies also contribute to the discrepancies in C_4F_7N/CO_2 decomposition characteristics. While computations based on transition-state theory (TST), Gibbs free energy minimization, and Chapman–Enskog theory have derived useful parameters of reaction rate constants, equilibrium compositions, thermodynamic properties, transport properties, and emission coefficients, they generally resulted in a great number of decomposition species/possibilities that did not match the experimental observations.[19–23]

In this work, instead of examining the excessive possibilities of C_4F_7N/CO_2 decomposition, we focus on three fundamental propositions of C_4F_7N/CO_2 decompositions, namely, the most probable first step of an ideal C_4F_7N thermal decomposition, the likelihood of C_4F_7N decomposing into C_3F_6 and C_2N_2 at low temperatures and the associated catalyst-assisted C_4F_7N cracking mechanism, as well as the preference of product generation in C_4F_7N decomposition by electrical discharge, with an attempt to resolve the discrepancies in C_4F_7N/CO_2 decompositions reported in the literature. In accordance with computations, C_4F_7N/CO_2 decomposition experiments were conducted, which include pyrolysis, long-term thermal aging with and without a catalytic material, and electrical spark discharge decomposition. Signatures of decomposition products in representative decomposition scenarios were extracted. Although by no means are our computations and experiments considered thorough or all-inclusive, this work marks the first step toward validated interpretations of the complicated C_4F_7N/CO_2 decompositions with a clear classification of their characteristics.

II. COMPUTATIONAL METHODS

A. Transition-state theory (TST)

According to the Born–Oppenheimer (BO) approximation, the electronic energy of a molecule at the ground state is a function that depends only on the coordinates of the nucleus.[24] The electronic energy of the molecule, thus, can be viewed as a hypersurface, namely, the potential energy surface (PES).[25] On the PES of a reaction, the intrinsic reaction coordinate (IRC) is the minimum energy reaction pathway (MERP) in mass-weighted Cartesian coordinates between the transition state (TS) of a reaction and its reactants and products, where the TS is located at the first order saddle point on the PES. Based on the transition-state theory (TST), a reaction is mediated by the formation of an activated complex, namely, the TS of the reaction, and the decomposition of that complex into the reaction products.[26,27] The forward rate constant of a reaction can be expressed as

$$k_f(T) = \kappa\sigma\frac{k_b T}{h}\left(\frac{RT}{P_0}\right)^{\Delta n} e^{-\frac{\Delta G^{\ddagger}}{RT}}, \tag{1}$$

where $k_f(T)$ is the forward rate constant as a function of temperature T, κ is the vibrational scaling factor, σ is the reaction path degeneracy, k_b is Boltzmann's constant, h is Planck's constant, R is the ideal gas constant, P_0 is the standard pressure, and $\Delta G^{\ddagger}$ is the standard Gibbs free energy of forming the TS. Here, $\Delta n = 1$ or 0 is for gas-phase bimolecular or unimolecular reactions, respectively.

The reaction path degeneracy σ can be obtained using the following formula:

$$\sigma = \sigma(R)n(R)/[\sigma(TS)n(TS)], \tag{2}$$

where $\sigma(R)$ and $\sigma(TS)$ are the numbers of rotational symmetries of the reactants and the transition states, respectively, while $n(R)$ and $n(TS)$ are the numbers of chiral isomers of the reactants and the transition states, respectively.

The equilibrium constant K_c of a reaction can be obtained using

$$K_c = e^{\frac{\Delta S^0}{R} - \frac{\Delta H^0}{RT}}, \tag{3}$$

where ΔS^0 and ΔH^0 refer, respectively, to the change of entropy in the complete transformation from reactants to products in the reaction.

Then, the reverse rate constant of the reaction can be obtained using

$$k_r = \frac{k_f}{K_c}. \tag{4}$$

For reactions with intrinsic barriers, the TS searching in this work was carried out by performing a Newton–Raphson search on the PES. Activation energies of these reactions with intrinsic

barriers are normally lower than the energies needed for the bond dissociations in reactants, because while bonds are being broken, the bonds that need to be formed in the products are simultaneously being created.

For reactions without intrinsic barriers (barrierless reactions), which are often encountered in bond dissociation reactions, an accurate calculation of reaction rate constants is still challenging, since the potential energy of these reactions tends to increase monotonically as the bond breaks.[28,29] In principle, more quantitative results can be obtained using methods like the variable-reaction coordinate variational transition-state theory (VRC-VTST) by minimizing the rate constant with respect to the location of a generalized TS for each total energy E and total angular momentum J, but a significant computational cost can be incurred.[30,31]

Nevertheless, since in a bond dissociation reaction, while the bond is being broken, no bond is simultaneously being created, the activation energy of a bond dissociation reaction is close to the bond energy of the bonds to be dissociated in the reactant. In this sense, to simplify the calculation of the rate constant of a bond dissociation reaction and for qualitative comparison only, we chose the Gibbs free energy difference between the reactant and the products (two separated free radicals) as the Gibbs free energy of activation.

Computations described in this section were performed with Gaussian 09 at the M062x/6-311G** level.

B. Chemical kinetic model

The composition of a system undergoing chemical reactions can be investigated using methods of chemical kinetics. In a chemical kinetic model, given that there are K chemical species in a system, reactions can be presented in the general form of

$$\sum_{k=1}^{K} \nu_{kif} m_k \langle = \rangle \sum_{k=1}^{K} \nu_{kir} m_k, \tag{5}$$

where ν_{kif} and ν_{kir} are the stoichiometric coefficients of a reaction and m_k is the chemical symbol for the kth species. The production rate w_k of the kth species can be expressed as a summation of the rates of progress variables for all reactions involving the kth species,

$$w_k = \sum_{i=1}^{I} \nu_{ki} q_i, \tag{6}$$

where

$$\nu_{ki} = \nu_{kif} - \nu_{kir}, \tag{7}$$

$$q_i = k_{fi} \prod_{k=1}^{K} [X_k]^{\nu_{kif}} - k_{ri} \prod_{k=1}^{K} [X_k]^{\nu_{kir}}, \tag{8}$$

in which X_k is the molar concentration of the kth species and k_{fi} and k_{ri} are the forward and reverse reaction rate constants of the ith reaction, respectively.

In this work, computations related to the chemical kinetics of C_4F_7N decomposition were carried out using Ansys Chemkin.

C. Qualitatively probing the composition and product generation of C_4F_7N non-thermal plasma

While the composition of thermal plasma, typically generated by arcs, can be probed by minimizing the Gibbs free energy of the system,[32–34] the composition of non-thermal plasma, typically generated by non-arc discharges, cannot be probed by the same method since non-thermal plasma is not in a state of equilibrium both chemically and thermally.

Theoretically, the composition of non-thermal plasma can be quantitatively obtained by solving Boltzmann's equation, which is not easy even with proper approximations that can reduce the equation. In non-thermal plasma, electrons are the only component that causes inelastic collisions with atoms and molecules, leading to excitation, dissociation, or ionization,[35] and it is reasonable to assume that electron impact is the main cause of gas decomposition. Because weaker bonds are generally more vulnerable to electron impacts, qualitatively, the plasma composition and the preference for product generation in non-thermal plasma should be highly related to the bond strengths of gas molecules.

In this work, the C_4F_7N plasma compositions and the preference of product generation in C_4F_7N electrical decomposition by discharge were qualitatively discussed with respect to the bond strengths of C_4F_7N. We characterized the bond strengths of C_4F_7N using the relaxed force constants of bonds,[36–38] which offers advantages over methods based on bond length or bond energy computations, as bond lengths can be used only when comparing the strengths of the same type of bonds, and bond energies may be affected by the deformation energies of molecular fragments. Computations to obtain the relaxed force constants of the bonds of C_4F_7N were performed with Gaussian 09 at the M062x/6-311G** level.

III. EXPERIMENTAL DETAILS

To verify the computational results, three types of C_4F_7N/CO_2 decomposition experiments were conducted, such as pyrolysis at 800 °C, long-term thermal aging with and without catalytic materials at 100 °C, and electrical decomposition by periodic spark discharges at 15.5 kV (~12 J/spark discharge at 0.1 Hz for 48h). C_4F_7N/CO_2 gas mixture samples used in the above decomposition and aging experiments were mixed at a ratio of 2:8. C_4F_7N/CO_2 gas mixtures at such a ratio display insulation performance nearly equivalent to that of SF_6.[39] In anticipation of comparing the decomposition characteristics of C_4F_7N/CO_2 gas mixtures with that of SF_6 on an equal-performance basis in future work, we chose this ratio for conducting the C_4F_7N/CO_2 decomposition experiments. After each experiment, 50 μl of each post-experiment C_4F_7N/CO_2 gas mixture sample was extracted for gas chromatography–mass spectrometry (GC–MS) analysis (Agilent 7890/5975).

The C_4F_7N/CO_2 pyrolysis experiment was conducted and analyzed with the pyrolysis GC–MS in a quartz tube furnace heated to 800 °C. The pyrolysis time in the quartz tube furnace was 1 min. Decomposition products after the pyrolysis were separated and analyzed by using the GC–MS downstream. A detailed description of the pyrolysis GC–MS can be found in the literature.[40,41]

The C_4F_7N/CO_2 long-term thermal aging experiment with/without catalytic materials was conducted with sealed glass cells of approximately 1 l, filled with C_4F_7N/CO_2 gas mixture samples at 1.2 bar. In the long-term thermal aging experiment, 30 g of molecular sieves 4A (Hi-dry® 4A, Multisorb Filtration Group), as a commonly used desiccant and adsorbent in gas-insulated apparatuses, was selected as the "catalytic" material to age with the C_4F_7N/CO_2 gas mixture sample. Sealed glass cells containing the C_4F_7N/CO_2 gas mixtures with/without the catalytic material were put in an oven for aging at 100 °C for six months. After aging, aged C_4F_7N/CO_2 gas mixture samples were extracted and analyzed with GC–MS.

The C_4F_7N/CO_2 electrical decomposition by periodical spark discharges was conducted by using a sealed glass chamber of approximately 0.5 l, where a pair of rod-to-plate electrodes made of brass was embedded. The diameter of the rod electrode was 2 mm, of which the top is chamfered. The distance between the rod electrode and the plate electrode was 1 mm. Spark discharges periodically triggered between this pair of electrodes were powered by a 15.5 kV capacitor bank of 0.1 μF, where 8 s was used for charging the capacitor bank and 2 s was allowed for its discharging. The C_4F_7N/CO_2 electrical decomposition by periodical spark discharges lasted for 48h, during which a total of 17 000 sparks were triggered in the testing chamber.

IV. COMPUTATIONAL RESULTS

A. The most probable first step of an ideal C_4F_7N thermal decomposition

Considering the extremely high strength of most triple bonds, direct dissociation of the triple bond of the nitrile group (C≡N) in C_4F_7N as the first step of an ideal C_4F_7N thermal decomposition is highly unlikely. Therefore, if only the homolysis of single bonds in C_4F_7N is considered, there are four possible first steps of an ideal C_4F_7N thermal decomposition, as shown in Fig. 1(a). The first possibility refers to the bond dissociation between —CN and $—C_3F_7$ in C_4F_7N. The second possibility refers to the bond dissociation between $—CF_3$ and $—C_3F_4CN$ in C_4F_7N. The third and fourth possibilities refer to the detachment of fluorine atoms from two different positions in the C_4F_7N molecule, respectively.

Figure 1(b) shows the calculated forward reaction rate constants of these four possible first steps. As shown in Fig. 1(b), two fluorine-atom-detachment reactions, regardless of the position of the fluorine atom to be detached from, have the lowest forward reaction rate constants, which is consistent with the general observation that the carbon-fluorine (C—F) bond is one of the strongest single bonds in chemistry. The forward rate constant of the bond dissociation between —CN and $—C_3F_7$ is higher than that of two fluorine-atom-detaching reactions, but is still significantly lower than that of the bond dissociation between $—CF_3$ and $—C_3F_4CN$ in C_4F_7N, suggesting that the bond dissociation reaction $C_4F_7N \rightarrow C_3F_4CN\cdot + CF_3\cdot$ [possibility 2 in Fig. 1(a)] is the most probable first step of an ideal C_4F_7N thermal decomposition.

Following the bond dissociation reaction $C_4F_7N \rightarrow C_3F_4CN\cdot + CF_3\cdot$ [possibility 2 in Fig. 1(a)], C_4F_7N molecules decompose into $C_3F_4CN\cdot$ free radicals and $CF_3\cdot$ free radicals.

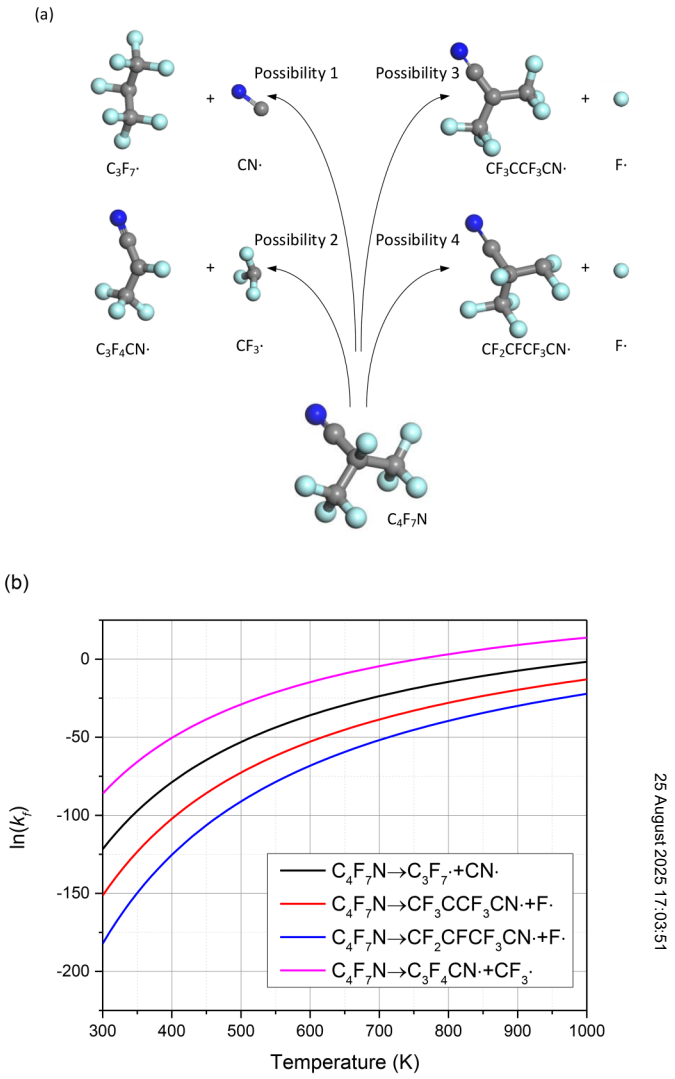

FIG. 1. (a) Four possible first steps of an ideal C_4F_7N thermal decomposition. (b) Calculated forward reaction rate constants of these four possible first steps.

A part of the $CF_3\cdot$ free radicals generated may then recombine with the $C_3F_4CN\cdot$ free radicals to form back C_4F_7N molecules, and the remaining $CF_3\cdot$ free radicals may recombine with themselves to form C_2F_6. For those $C_3F_4CN\cdot$ free radicals not recombined with $CF_3\cdot$ free radicals, they may either recombine with themselves to form perfluorinated dinitriles with large molecular weights, which are likely to condense as liquid or solid that cannot be detected in the gas phase, or further decompose and evolve into small fluoronitriles that are likely to be detected in the gas phase. Therefore, based on the computational results above, the main gaseous decomposition products at the early stage of an ideal C_4F_7N thermal decomposition should be C_2F_6 and small fluoronitriles.

B. The likelihood of C_4F_7N decomposing into C_3F_6 and C_2N_2 at low temperatures and the associated catalyst-assisted C_4F_7N cracking mechanism

Computations in the last section suggested that C_4F_7N is likely to decompose first into C_2F_6 and small fluoronitriles in an ideal thermal decomposition. However, in several thermal decomposition experiments, C_4F_7N was reported to be first decomposed and cracked into C_3F_6 and C_2N_2 at low temperatures.[18] To probe the likelihood of C_4F_7N decomposing into C_3F_6 and C_2N_2 at low temperatures, the corresponding decomposition pathway must be developed first. Among various possible pathways through which C_4F_7N decomposes into C_3F_6 and C_2N_2, we chose the pathway shown in Fig. 2 as the pathway of investigation, since following this pathway, C_4F_7N decomposes into C_3F_6 and C_2N_2 in the least number of steps.

The decomposition pathway shown in Fig. 2 starts with the bond dissociation reaction of a C_4F_7N molecule decomposing into a CN· free radical and a C_3F_7· free radical with a remarkable electronic energy barrier (100.34 kcal/mol). After this bond dissociation reaction, two CN· free radicals recombine with each other to form a C_2N_2 molecule. On the other hand, the C_3F_7· free radical further decomposes and evolves into C_3F_6. The electronic energy barriers or releases of those steps are also shown in Fig. 2.

To form a C_3F_6 molecule from a C_3F_7· free radical, a fluorine atom must be further detached from the C_3F_7· free radical. Because fluorine atoms in the C_3F_7· free radical can be divided into two groups based on the symmetry of this free radical, there are two possible manners of fluorine atom detaching from this free radical, namely, $C_3F_7\cdot \rightarrow CF_2CFCF_3\cdot + F\cdot$ and $C_3F_7\cdot \rightarrow CF_3CCF_3\cdot + F\cdot$. As shown in Fig. 2, the reaction $C_3F_7\cdot \rightarrow CF_2CFCF_3\cdot + F\cdot$ has a relatively low electronic energy barrier (+62.53 kcal/mol), while the electronic energy barrier for the reaction $C_3F_7\cdot \rightarrow CF_3CCF_3\cdot + F\cdot$ is high (+132.97 kcal/mol).

In addition, there is a clear TS in the isomerization from the CF_3CCF_3· free radical to C_3F_6, posing a further electronic energy barrier (+7.348 kcal/mol). The presence of this TS indicates that, in this isomerization reaction, a structure with energy higher than both that of the reactant and that of the products exists, where the fluorine atom originally connecting to one of the two carbon atoms at the ends of the CF_3CCF_3· free radical is detached and bound to the carbon atom in the middle of the CF_3CCF_3· free radical.

After performing vibrational analysis on the species shown in Fig. 2, the Gibbs free energy of each species can be obtained. Then, using the TST described above, reaction rate constants can be calculated. The forward rate constants of the reactions of interest are shown in Fig. 3(a). As shown in Fig. 3(a), the rate constants of similar reactions demonstrate the same trend. To be specific, the rate constants of two isomerization reactions, namely,

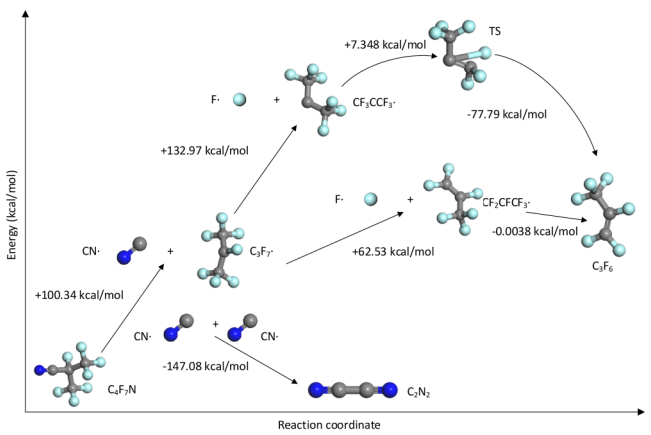

FIG. 2. The pathway of C_4F_7N decomposing into C_2N_2 and C_3F_6 in the least number of steps.

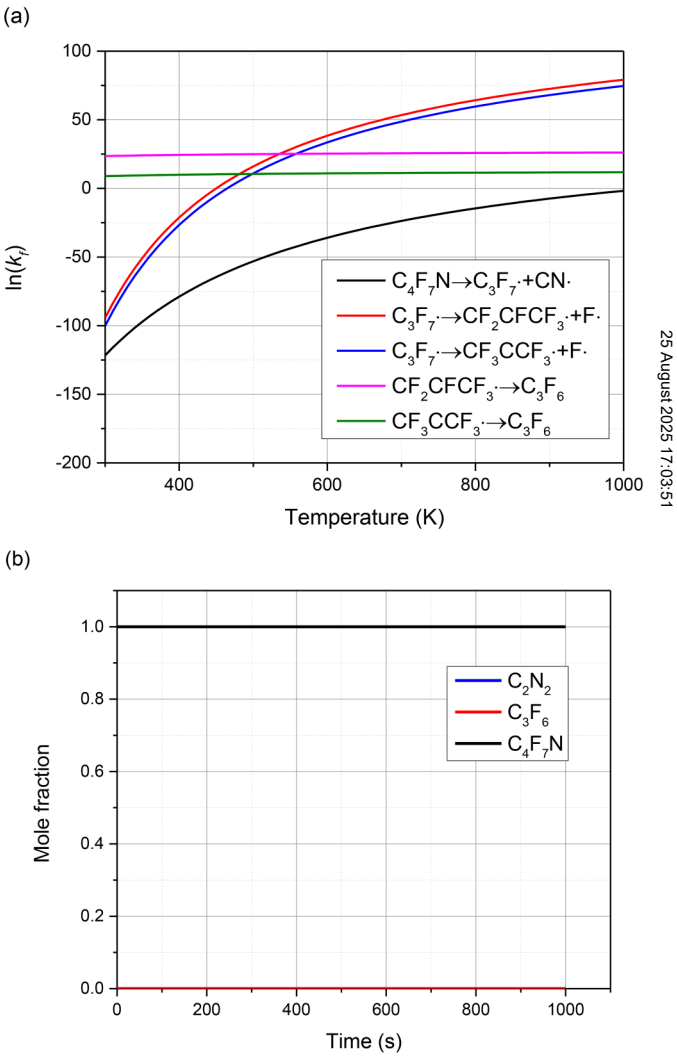

FIG. 3. (a) Forward reaction rate constants of steps. (b) The chemical kinetics of C_4F_7N decomposing into C_3F_6 and C_2N_2 at 650 K (377 °C) for 1000 s.

$CF_2CFCF_3\cdot \rightarrow C_3F_6$ and $CF_3CCF_3\cdot \rightarrow C_3F_6$, are both very high even at room temperatures and do not change significantly with temperature, while the rate constants of two fluorine-atom-detaching reactions, namely, $C_3F_7\cdot \rightarrow CF_2CFCF_3\cdot + F\cdot$ and $C_3F_7\cdot \rightarrow CF_3CCF_3\cdot + F\cdot$, are both extremely low at room temperatures but increase very fast as the temperature increases. The reaction $C_4F_7N \rightarrow C_3F_7\cdot + CN\cdot$ is a special one, as in the temperature range of investigation (300–1000 K), the forward rate constant of this reaction is always significantly lower than that of all others, suggesting that this reaction is the rate-determining step (RDS) of the reaction pathway shown in Fig. 2.

Using the reaction rate constants calculated, a chemical kinetic model of C_4F_7N decomposing into C_3F_6 and C_2N_2 at 650 K (377 °C) can be set up. A temperature of 650 K is close to the literature-reported temperature for the thermal decomposition of C_4F_7N into C_3F_6 and C_2N_2, i.e., ∼350 °C.[18] The result of this chemical kinetic model, as shown in Fig. 3(b), demonstrates that, at 650 K, due to the extremely low forward reaction rate of the RDS ($C_4F_7N \rightarrow C_3F_7\cdot + CN\cdot$), after a sufficiently long time (1000 s), almost no C_3F_6 and C_2N_2 is generated, and almost no C_4F_7N is decomposed, suggesting that the likelihood of direct generation of C_3F_6 and C_2N_2 from C_4F_7N at low temperatures is very low. For these thermal decomposition experiments where C_4F_7N was first decomposed and cracked into C_3F_6 and C_2N_2 at low temperatures, catalytic materials that can significantly lower the activation energy of the RDS ($C_4F_7N \rightarrow C_3F_7\cdot + CN\cdot$) must be present.

C. The preference of product generation in C_4F_7N decomposition by electrical discharge

As discussed above, electron impact is likely to be the main cause of C_4F_7N electrical decomposition by discharge. In principle, as long as the electron impact is of high enough energy, all bonds in C_4F_7N can be dissociated; however, stronger bonds are generally more resistant to an electron impact event. The plasma composition and preference of product generation in this decomposition scenario should, thus, be highly related to the bond strengths of C_4F_7N.

Figure 4(a) shows the relaxed force constants of the bonds in C_4F_7N. A greater relaxed force constant corresponds to a stronger bond strength. As shown in Fig. 4(a), the bond between C1 and C2 atoms and the bond between C2 and C4 atoms are the weakest bonds in C_4F_7N. Because CF_3 fragments (neutrals and ions) can be generated by breaking either one of these two bonds as well as by simultaneously breaking these two bonds, CF_3 fragments should be the dominant component of electron-impact-induced C_4F_7N non-thermal plasma, assuming that the energy of electron impact is not high enough to dissociate most CF_3. In contrast, since small fluoronitrile fragments can be generated only by breaking either the C1—C2 bond or the C2–C4 bond, small fluoronitrile fragments in this C_4F_7N non-thermal plasma should be less than CF_3 fragments.

The bond between the C2 and the C3 atoms and the C—F bonds in C_4F_7N is stronger than the C1—C2 bond and the C2—C4 bond, and the dissociations of the C2—C3 bond and the C—F bonds generate CN fragments and F fragments. Due to the strengths of the C2—C3 bond and the C—F bonds, CN fragments and F fragments resulting from the dissociations of these two

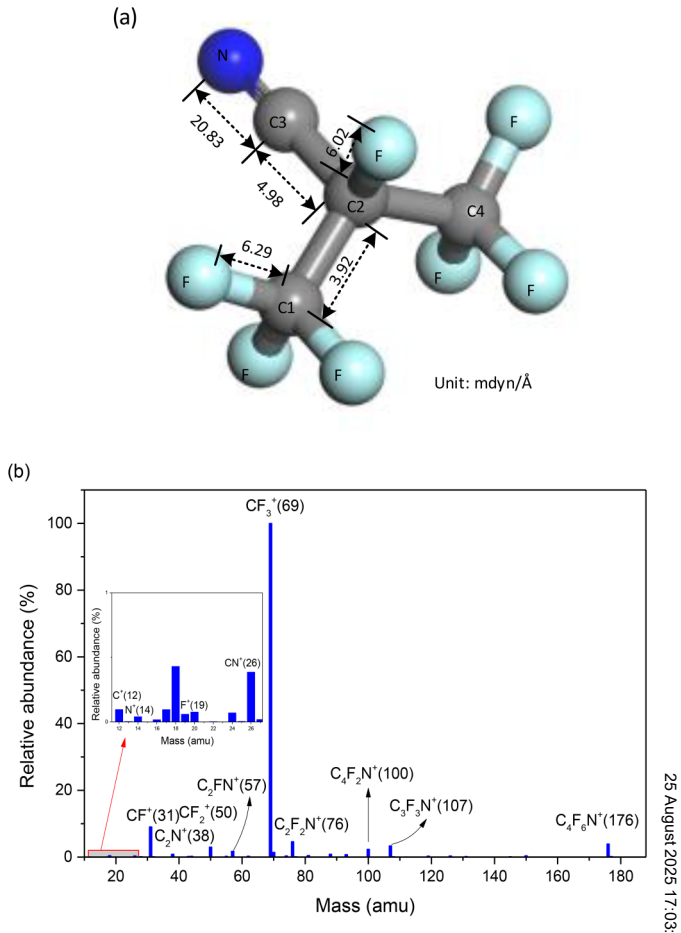

FIG. 4. (a) Relaxed force constants of the bonds in C_4F_7N. (b) The mass spectrum of C_4F_7N generated by electron impact at 70 eV.

bonds should have lower abundances than that of CF_3 or small fluoronitrile fragments.

As can be seen from Fig. 4(a), the strongest bond in C_4F_7N is the bond between the N and the C3 atoms. Therefore, the dissociation of the N—C3 bond in C_4F_7N electrical decomposition by discharge should be minor. Because N fragments can be generated only by the dissociation of the N—C3 bond, N fragments should be the least among all plasma components.

Figure 4(b) shows the mass spectrum of C_4F_7N generated by electron impact at 70 eV, which verifies the analysis above. In this C_4F_7N mass spectrum, CF_3 fragments are the dominant component, followed by small fluoronitrile fragments. CN and F fragments can also be observed but are of far less abundance. N fragments are of the least abundance. It should be noted that 70 eV is way above the ionization thresholds of possible fragments of C_4F_7N,[42–45] and, therefore, most of the fragments of C_4F_7N generated at this electron energy level are expected to be positive ions.

C_4F_7N non-thermal plasma extinguishes immediately after electrical discharge in C_4F_7N gas mixtures, where free electrons

and C_4F_7N fragments including ions and neutrals recombine with each other to form decomposition products. With the abundance of these fragments as precursors of C_4F_7N aging products from high to low being that of CF_3, fluoronitriles, CN, F, and N, and with the assumption that precursors of high abundance generate products of high concentrations, it can be expected that after C_4F_7N electrical decomposition by discharge, C_2F_6 and fluoronitriles are the major products, and small molecule products like CF_4 and C_2N_2 are at low concentrations if they can be detected.

V. EXPERIMENTAL RESULTS

Figures 5(a)–5(d) show, respectively, the compositions of post-experiment gas samples from the C_4F_7N/CO_2 pyrolysis at 800 °C, the C_4F_7N/CO_2 decompositions after six-month thermal aging with/without a catalytic material (industrial-grade molecular sieves 4A) at 100 °C, and the C_4F_7N/CO_2 electrical decomposition by spark discharges at 15.5 kV for 48h (a total of 17 000 sparks).

For C_4F_7N/CO_2 pyrolysis, a significant thermal decomposition of C_4F_7N with a quartz tube furnace can be observed only after pyrolysis at high temperatures, e.g., ~800 °C. As shown in Fig. 5(a), the main gaseous decomposition products after C_4F_7N/CO_2 pyrolysis at 800 °C include CO, C_2F_6, COF_2, C_3F_6, and various small fluoronitriles. Among the fluorinated decomposition products resulting from C_4F_7N decomposition, the concentration of C_2F_6 is the highest, followed by that of those various small fluoronitriles added together. Within the resolution of our instrumentation, we did not detect small molecules like CF_4 and C_2N_2.

Figures 5(b) and 5(c) show the compositions of post-experiment gas samples from the C_4F_7N/CO_2 six-month thermal

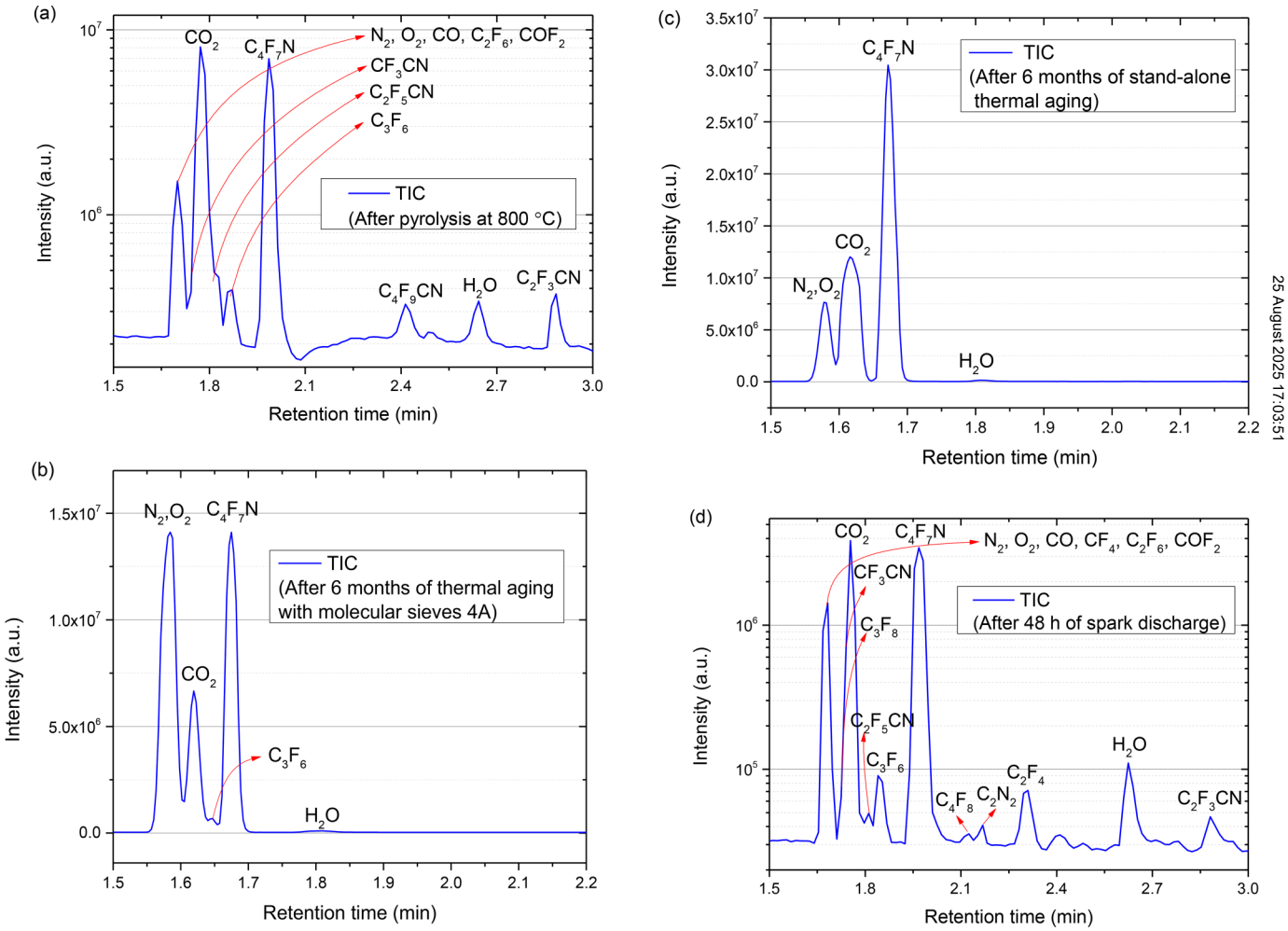

FIG. 5. Compositions of post-experiment gas samples from (a) the C_4F_7N/CO_2 pyrolysis at 800 °C, the C_4F_7N/CO_2 six-month thermal aging (b) with/(c) without a catalytic material (industrial-grade molecular sieves 4A) at 100 °C, (d) the C_4F_7N/CO_2 electrical decomposition by periodical spark discharges for 48h at 15.5 kV with a repetition rate of 0.1 Hz. TIC stands for the total ion current of GC–MS.

aging with/without molecular sieves 4A at 100 °C. As shown in Fig. 5(b), with molecular sieves 4A, after six months of thermal aging at 100 °C, a part of C_4F_7N was decomposed into C_3F_6. In the meantime, CN free radicals released from C_4F_7N decomposition are likely to form C_2N_2. However, with such a small size and linear structure of C_2N_2, C_2N_2 can be easily adsorbed by molecular sieves 4A, making C_3F_6 the only decomposition product that can be detected in the gas phase. In contrast, as shown in Fig. 5(c), without molecular sieves 4A, after six months of thermal aging at 100 °C, no C_4F_7N decomposition was detected. The above experimental results suggest that C_4F_7N remains stable at 100 °C, and the reaction of C_4F_7N decomposing into C_3F_6 at this temperature was "catalyzed" by the industrial-grade molecular sieves 4A. In other words, the —CN group appears to be the site chemically active to "catalytic" materials, e.g., the co-mineral residuals of the metakaolin used in the synthesis of industrial-grade molecular sieves 4A.

As shown in Fig. 5(d), after 48h of spark discharges aging at 15.5 kV, C_4F_7N/CO_2 electrical decomposition generates significantly more species of decomposition products than thermal decomposition. While C_2F_6 and small fluoronitriles are still the main decomposition products after this experiment, other species of small molecules like CF_4 and C_2N_2 of low concentrations can also be detected.

The experimental observations above generally agree with the conclusions and inferences from our computations presented in this work. In addition, they form a solid basis to resolve the discrepancies in the literature reporting the C_4F_7N/CO_2 decomposition characteristics. For instance, Kieffel *et al.* reported that C_4F_7N/CO_2 started to decompose at 650 °C, and the main decomposition products were C_2F_6 and small fluoronitriles with no CF_4 and C_2N_2,[13] which is generally in line with the results of our C_4F_7N/CO_2 pyrolysis experiment and our computational study of the most probable first step of an ideal C_4F_7N thermal decomposition. Both Kieffel's and our studies used a quartz tube furnace as the decomposition reactor, which is chemically inert to most compounds. The C_4F_7N/CO_2 thermal decomposition characteristics revealed herein are thus considered more related to the intrinsic thermodynamic stability of C_4F_7N molecules.

Zhang *et al.* reported that in their C_4F_7N/CO_2 thermal decomposition experiments, C_3F_6 appeared as the first decomposition product at only 350 °C, and then C_2N_2 started to appear at a slightly higher temperature.[18] The heater in their experiments was made of copper, and copper can react with C_4F_7N first to produce metal cyanides and C_3F_6 at lower temperatures.[46] The C_4F_7N/CO_2 thermal decomposition characteristics revealed in their experiments were analogous to our C_4F_7N/CO_2 six-month thermal aging experiments with industrial-grade molecular sieves 4A at 100 °C, both suggesting that the -CN group in C_4F_7N is chemically active to certain catalytic materials.

Chen *et al.* and Li *et al.* conducted C_4F_7N/CO_2 electrical decomposition experiments with different experimental configurations and conditions,[16,20] and they both reported C_4F_7N/CO_2 electrical decomposition characteristics very similar to the characteristics revealed in our periodic spark discharge experiment. Generally, more species of decomposition products can be detected after C_4F_7N/CO_2 electrical decomposition than after C_4F_7N/CO_2 thermal decomposition, but the main decomposition products after C_4F_7N/CO_2 electrical decomposition were still C_2F_6 and small fluoronitriles. Decomposition products of small molecules like CF_4 and C_2N_2 can be detected after C_4F_7N/CO_2 electrical decomposition, but the concentrations of CF_4 and C_2N_2 are much lower than those of C_2F_6 and small fluoronitriles. These experimental observations of C_4F_7N/CO_2 electrical decomposition feature the characteristics of decomposition product generation from electron-impact-induced non-thermal C_4F_7N plasma.

Based on our computational and experimental studies, C_4F_7N/CO_2 decomposition characteristics can then be categorized into three groups, namely, ideal thermal decomposition, thermal decomposition in the presence of catalytic materials, and electrical decomposition by discharge, corresponding to different C_4F_7N/CO_2 decomposition scenarios. Signatures of C_4F_7N decomposition products in these decomposition scenarios were extracted and are summarized in the Venn diagram shown in Fig. 6.

The N_2 and O_2 shown in Fig. 5 were caused by the tiny air that inevitably got mixed during the transfer of post-experiment samples, and, therefore, they should not be counted as decomposition products. The presence of CO and COF_2 after C_4F_7N/CO_2 thermal decomposition and electrical decomposition suggests that during the decomposition, CO_2 first decomposes into CO and O free radicals, and O free radicals may recombine with CF_2· free radicals to generate COF_2. CO and COF_2 as C_4F_7N/CO_2 decomposition products were also reported in the literature.[13]

In addition, it must be emphasized that the decomposition experiments above were highly accelerated under extreme conditions within small volumes (~1 l) so that the decomposition characteristics of C_4F_7N/CO_2 gas mixtures can be more prominently demonstrated. In real-world applications, the decomposition of C_4F_7N/CO_2 gas mixtures is expected to be much more moderate. As a supplement to this study, we conducted an arc decomposition

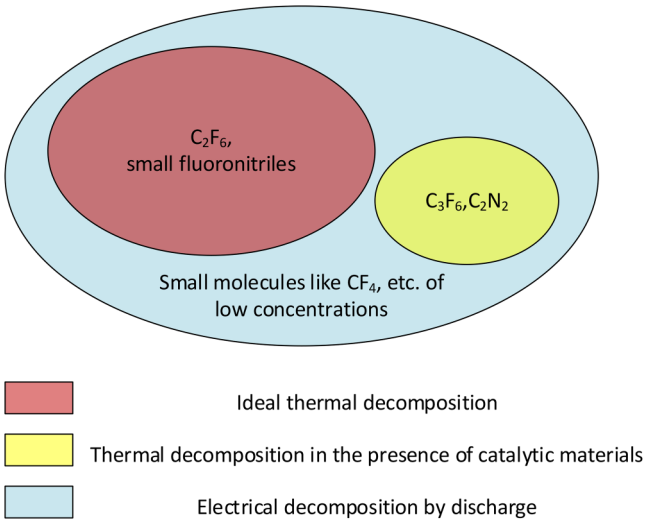

FIG. 6. Signatures of C_4F_7N decomposition products in different decomposition scenarios.

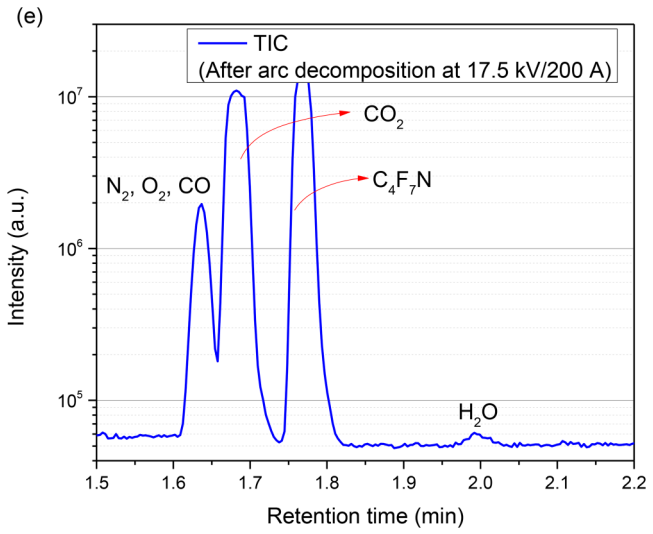

FIG. 7. The composition of the post-experiment gas sample after one shot of arc decomposition in a real C_4F_7N/CO_2 filled-load disconnector at 17.5 kV/200 A.

experiment using a real C_4F_7N/CO_2 (2:8)-filledload disconnector at 1.65 bar with an 85 l volume. After one shot of arc at 17.5 kV and 200 A, the concentrations of the decomposition products were so low that they could not be picked up by our GC–MS, as shown in Fig. 7, suggesting that throughout the service lives of typical circuit breakers (~100 times of operations), running out of C_4F_7N due to decomposition is highly unlikely.

It also should be pointed out that a considerable accumulation of both gaseous and solid decomposition byproducts was also observed in the SF_6-filled power equipment. The formation rates of SF_6 decomposition byproducts have been quantified, and suitable adsorbents have been developed to mitigate the accumulation of SF_6 decomposition byproducts.[1,47] These efforts have contributed to the progressive maturity of SF_6 insulation technology over the decades. In the future, to advance the technology readiness level (TRL) of C_4F_7N insulation, research focusing on the quantification of C_4F_7N decomposition rates, as well as the identification of effective adsorbents for C_4F_7N decomposition byproducts, should also be undertaken.

VI. CONCLUSIONS

In this work, the decomposition characteristics of C_4F_7N/CO_2 gas mixtures as a promising SF_6 alternative were studied comprehensively by both computations and experiments. Starting from fundamental propositions of C_4F_7N/CO_2 decomposition, meaningful conclusions and inferences were derived. The first step of an ideal C_4F_7N thermal decomposition is likely to be $C_4F_7N \rightarrow C_3F_4CN\cdot + CF_3\cdot$, followed by the formation of C_2F_6 and small fluoronitriles as the main gaseous decomposition products in the early stage of an ideal C_4F_7N thermal decomposition. The reaction of C_4F_7N decomposing into C_3F_6 and C_2N_2 at lower temperatures appears possible only in the presence of incompatible (catalytic) materials that can significantly lower the activation energy of the RDS ($C_4F_7N \rightarrow C_3F_7\cdot + CN\cdot$). While C_2F_6 and small fluoronitriles continue to be the main productions of C_4F_7N/CO_2 electrical decomposition by discharge, other species of small molecules like CF_4 and C_2N_2 of low concentrations may also be present in C_4F_7N/CO_2 electrical decomposition.

The aforementioned C_4F_7N/CO_2 decomposition characteristics were experimentally validated by pyrolysis, long-term thermal aging with and without a catalytic material (e.g., industrial-grade molecular sieves 4A), and electrical decomposition with spark discharge, which were all in good agreement with the computations. The possible cracking of C_4F_7N/CO_2 in the presence of incompatible (catalytic) materials strongly suggests that care must be taken when selecting materials for new switchgear design. Low-energy spark or corona discharge appears to form most types of species because of the non-equilibrium nature of electron-impact-induced decomposition in non-thermal plasma. Proper high-voltage designs will have to be considered in future SF_6-free power apparatuses.

Beyond these early identifications of dominant byproducts, there is a critical need to quantitatively determine the formation rates of C_4F_7N decomposition byproducts in various modes of electrical discharges, particularly in high-current arcs. Nonetheless, the decomposition of C_4F_7N/CO_2 in real applications will be at a much moderate rate than what is obtained from the highly accelerated laboratory tests presented in this work, and the risk of running out of C_4F_7N throughout the service lives of circuit breakers seems minimal. Furthermore, it is less likely that products resolved from low-energy spark aging can survive high-current interrupting arcs without further decomposition. With additional work, a thorough understanding of the decomposition characteristics of C_4F_7N/CO_2 can lead to the development of decomposition diagnostic tools as well as selective adsorbents for the removal and fixation of unwanted decomposition byproducts, facilitating the transition toward a green, SF_6-Free power network.

ACKNOWLEDGMENTS

The authors from the University of Connecticut and GE Global Research Center would like to acknowledge U.S. Department of Energy (DOE), Advanced Research Projects Agency–Energy (ARPA-e), for providing funding support to their work under Contract No. DE-AR0001523.

AUTHOR DECLARATIONS

Conflict of Interest

The authors have no conflicts to disclose.

Author Contributions

Wenqiang Gao: Conceptualization (supporting); Data curation (equal); Formal analysis (equal); Funding acquisition (supporting); Investigation (equal); Methodology (equal); Project administration (equal); Resources (equal); Software (equal); Supervision (equal); Validation (equal); Visualization (equal); Writing – original draft (lead); Writing – review & editing (equal). **Luisa Posada:** Investigation (supporting); Resources (supporting); Writing – review

& editing (supporting). **Vahid Shiravand:** Investigation (supporting); Writing – review & editing (supporting). **Shubhashish Shubhashish:** Investigation (supporting); Resources (supporting); Writing – review & editing (supporting). **Capri Price:** Investigation (supporting); Writing – review & editing (supporting). **Boya Zhang:** Investigation (supporting); Methodology (supporting); Resources (supporting); Writing – review & editing (supporting). **Radislav Potyrailo:** Investigation (supporting); Writing – review & editing (supporting). **Karim Younsi:** Investigation (supporting); Writing – review & editing (supporting). **Shiyao Shan:** Investigation (supporting); Writing – review & editing (supporting). **Ibrahima Ndiaye:** Investigation (supporting); Writing – review & editing (supporting). **Charlotte Cabrera:** Investigation (supporting); Writing – review & editing (supporting). **Jierui Zhou:** Investigation (supporting); Writing – review & editing (supporting). **Maxime Perret:** Writing – review & editing (supporting). **Thomas Berteloot:** Writing – review & editing (supporting). **Yannick Kieffel:** Writing – review & editing (supporting). **Andres Laso:** Investigation (supporting); Resources (supporting). **Nenad Uzelac:** Investigation (supporting); Resources (supporting). **Steven L. Suib:** Funding acquisition (supporting); Investigation (supporting); Resources (supporting); Supervision (supporting); Writing – review & editing (supporting). **Yang Cao:** Conceptualization (lead); Data curation (equal); Formal analysis (equal); Funding acquisition (lead); Investigation (lead); Methodology (equal); Project administration (equal); Resources (equal); Software (equal); Supervision (lead); Validation (equal); Visualization (equal); Writing – original draft (supporting); Writing – review & editing (lead).

DATA AVAILABILITY

The data that support the findings of this study are available from the corresponding author upon reasonable request.

REFERENCES

[1]D. Koch, "SF6 properties, and use in MV and HV switchgear," Cahier Technique No. 188, Schneider Electric, Collection Technique.

[2]E. A. Ray *et al.*, "Quantification of the SF_6 lifetime based on mesospheric loss measured in the stratospheric polar vortex," J. Geophys. Res. A **122**(8), 4626–4638, https://doi.org/10.1002/2016JD026198 (2017).

[3]M. Rigby *et al.*, "History of atmospheric SF_6 from 1973 to 2008," Atmos. Chem. Phys. **10**(21), 10305–10320 (2010).

[4]M. Maiss and C. A. Brenninkmeijer, "Atmospheric SF_6: Trends, sources, and prospects," Environ. Sci. Technol. **32**(20), 3077–3086 (1998).

[5]L. Niemeyer and F. Y. Chu, "SF_6 and the atmosphere," IEEE Trans. Electr. Insul. **27**(1), 184–187 (1992).

[6]M. Rabie and C. M. Franck, "Assessment of eco-friendly gases for electrical insulation to replace the most potent industrial greenhouse gas SF_6," Environ. Sci. Technol. **52**(2), 369–380 (2018).

[7]J. C. Devins, "Replacement gases for SF_6," IEEE Trans. Electr. Insul. **EI-15**(2), 81–86 (1980).

[8]R. E. Wootton and M. R. Kegelman, *Gases Superior to SF_6 for Insulation and Interruption* (Electric Power Research Insititute (EPRI), 1982), p. EL-2620.

[9]J. Owens *et al.*, "Recent development of two alternative gases to SF_6 for high voltage electrical power applications," Energies **14**(16), 5051 (2021).

[10]J. G. Owens, "Greenhouse gas emission reductions through use of a sustainable alternative to SF_6," in *2016 IEEE Electrical Insulation Conference (EIC)* (IEEE, 2016).

[11]Y. Kieffel *et al.*, "Green gas to replace SF_6 in electrical grids," IEEE Power Energy Mag. **14**(2), 32–39 (2016).

[12]A. Chachereau, A. Hösl, and C. M. Franck, "Electrical insulation properties of the perfluoronitrile C_4F_7N," J. Phys. D: Appl. Phys. **51**(49), 495201 (2018).

[13]Y. Kieffel, "Characteristics of g3—An alternative to SF_6," in *2016 IEEE International Conference on Dielectrics (ICD)* (IEEE, 2016), Vol. 2.

[14]S. Blázquez *et al.*, "Reaction kinetics of $(CF_3)_2CFCN$ with OH radicals as a function of temperature (278–358 K): A good replacement for greenhouse SF_6?," Chem. Phys. Lett. **687**, 297–302 (2017).

[15]M. P. Sulbaek Andersen *et al.*, "Atmospheric chemistry of $(CF_3)_2CF\text{-}C{\equiv}N$: A replacement compound for the most potent industrial greenhouse Gas, SF_6," Environ. Sci. Technol. **51**(3), 1321–1329 (2017).

[16]I. Iddrissu *et al.*, "Gas decomposition and electrode degradation characteristics of a 20% C_3F_7CN and 80% CO_2 gas mixture for high voltage accelerators," High Voltage **6**(5), 750–759 (2021).

[17]W. Gao *et al.*, "Materials compatibility study of C_4F_7N/CO_2 gas mixture for medium-voltage switchgear," IEEE Trans. Dielectr. Electr. Insul. **29**(1), 270–278 (2022).

[18]Y. Li *et al.*, "Study on the thermal decomposition characteristics of C_4F_7N–CO_2 mixture as eco-friendly gas-insulating medium," High Voltage **5**(1), 46–52 (2020).

[19]L. Chen *et al.*, "Decomposition mechanism and kinetics of iso-C_4 perfluoronitrile (C_4F_7N) plasmas," J. Appl. Phys. **126**(16), 163303 (2019).

[20]B. Zhang *et al.*, "Decomposition characteristics of C_4F_7N/CO_2 mixture under AC discharge breakdown," AIP Adv. **9**(11), 115212 (2019).

[21]Y. Fu *et al.*, "Theoretical study of the decomposition mechanism of C_4F_7N," J. Phys. D: Appl. Phys. **52**(24), 245203 (2019).

[22]Y. Wu *et al.*, "Properties of C_4F_7N–CO_2 thermal plasmas: Thermodynamic properties, transport coefficients and emission coefficients," J. Phys. D: Appl. Phys. **51**(15), 155206 (2018).

[23]M. Gnybida, C. Ruempler, and V. R. T. Narayanan, "Radiative properties and numerical modeling of C_4F_7N–CO_2-O_2 thermal plasma," Plasma Phys. Technol. **6**(2), 144–147 (2019).

[24]J.-M. Combes, P. Duclos, and R. Seiler, "The Born-Oppenheimer approximation," in *Rigorous Atomic and Molecular Physics* (Springer, Boston, 1981), pp. 185–213.

[25]A. D. McNaught, *Compendium of Chemical Terminology* (Blackwell Science, Oxford, 1997), Vol. 1669.

[26]M. G. Evans and M. Polanyi, "Some applications of the transition state method to the calculation of reaction velocities, especially in solution," Trans. Faraday Soc. **31**, 875–894 (1935).

[27]P. Pechukas, "Transition state theory," Annu. Rev. Phys. Chem. **32**(1), 159–177 (1981).

[28]M. J. Pilling, "Radical-radical reactions," Annu. Rev. Phys. Chem. **47**(1), 81–108 (1996).

[29]J. Troe, "Limitations of variational transition state theory for barrierless radical–radical recombination reactions," Z. Phys. Chem. **218**(4), 457–468 (2004).

[30]J. L. Bao, X. Zhang, and D. G. Truhlar, "Barrierless association of CF_2 and dissociation of C_2F_4 by variational transition-state theory and system-specific quantum Rice–Ramsperger–Kassel theory," Proc. Natl. Acad. Sci. U.S.A. **113**(48), 13606–13611 (2016).

[31]D. G. Truhlar, B. C. Garrett, and S. J. Klippenstein, "Current status of transition-state theory," J. Phys. Chem. **100**(31), 12771–12800 (1996).

[32]A. B. Murphy, "Thermal plasmas in gas mixtures," J. Phys. D: Appl. Phys. **34**(20), R151 (2001).

[33]A. B. Murphy, "Transport coefficients of air, argon-air, nitrogen-air, and oxygen-air plasmas," Plasma Chem. Plasma Process. **15**, 279–307 (1995).

[34]O. Coufal, "Composition and thermodynamic properties of thermal plasma up to 50 kK," J. Phys. D: Appl. Phys. **40**(11), 3371 (2007).

[35]R. Hippler *et al.*, *Low Temperature Plasma Physics: Fundamental Aspects and Applications* (Wiley-VCH, 2001).
[36]J. Grunenberg, "III-defined concepts in chemistry: Rigid force constants vs. Compliance constants as bond strength descriptors for the triple bond in diboryne," Chem. Sci. **6**(7), 4086–4088 (2015).
[37]K. Brandhorst and J. Grunenberg, "How strong is it? The interpretation of force and compliance constants as bond strength descriptors," Chem. Soc. Rev. **37**(8), 1558–1567 (2008).
[38]K. Brandhorst and J. Grunenberg, "Efficient computation of compliance matrices in redundant internal coordinates from Cartesian Hessians for nonstationary points," J. Chem. Phys. **132**(18), 184101 (2010).
[39]See https://multimedia.3 m.com/mws/media/1132124O/3m-novec-4710-insulating-gas-tech-data-sheet.pdf for the technical data of C_4F_7N.
[40]M. Ezrin and G. Lavigne, "Analysis of silicone polymers at trace levels by pyrolysis gas chromatography/mass spectroscopy," in *Society of Plastics Engineers ANTEC, San Francisco, CA* (2002), pp. 2046–2050.
[41]M. Ezrin and G. Lavigne, "Gas chromatography/mass spectroscopy for plastics failure analysis," Eng. Failure Anal. **12**(6), 851–859 (2005).
[42]L. G. Christophorou and J. K. Olthoff, "Electron interactions with C_2F_6," J. Phys. Chem. Ref. Data **27**(1), 1–29 (1998).
[43]S. R. Hunter and L. G. Christophorou, "Electron attachment to the perfluoroalkanes n-C_N F_{2N+2} (N = 1–6) using high pressure swarm techniques," J. Chem. Phys. **80**(12), 6150–6164 (1984).
[44]L. G. Christophorou, J. K. Olthoff, and M. V. V. S. Rao, "Electron interactions with CF_4," J. Phys. Chem. Ref. Data **25**(5), 1341–1388 (1996).
[45]C. A. McDowell and J. W. Warren, "The ionization and dissociation of cyanogen and methyl cyanide by electron impact," Trans. Faraday Soc. **48**, 1084–1093 (1952).
[46]Y. Li *et al.*, "Thermal compatibility between perfluoroisobutyronitrile-CO_2 gas mixture with copper and aluminum switchgear," IEEE Access **7**, 19792–19800 (2019).
[47]F. Y. Chu, "SF_6 decomposition in gas-insulated equipment," IEEE Trans. Electr. Insul. **EI-21**(5), 693–725 (1986).